Desalination and Water Treatment
www.deswater.com

doi: 10.5004/dwt.2017.20205

63 (2017) 283–292
February

Co/TiO_2 nanoparticles: preparation, characterization and its application for photocatalytic degradation of methylene blue

Azadeh Ebrahimian Pirbazari[a,b,*], Pejman Monazzam[a,b], Behnam Fakhari Kisomi[b]

[a]*Fouman Faculty of Engineering, College of Engineering, University of Tehran, P.O. Box 43515-1155, Fouman 43516-66456, Iran, Tel. +981334734927; Fax: +981334737228; emails: aebrahimian@ut.ac.ir (A.E. Pirbazari), pmonazzam@ut.ac.ir (P. Monazzam)*
[b]*Caspian Faculty of Engineering, College of Engineering, University of Tehran, P.O. Box 43841-119, Rezvanshahr 43861-56387, Iran, Behnam_fakhari@ut.ac.ir*

Received 30 March 2016; Accepted 29 August 2016

ABSTRACT

In this work, TiO_2 nanoparticles containing different amounts of cobalt were synthesized by sol-gel method using titanium (IV) isopropoxide and cobalt chloride as titanium and cobalt precursors, respectively. X-ray diffraction (XRD) results showed prepared samples include 100% anatase phase. The presence of cobalt in TiO_2 nanoparticle network was established by XRD, scanning electron microscopy equipped with energy dispersive X-ray microanalysis (SEM-EDX), Fourier transform infrared (FT-IR) and N_2 physisorption techniques. The increase of cobalt doping enhanced redshift in the diffuse reflectance spectra. The photocatalytic activity of the prepared samples was tested for degradation of methylene blue (MB) as a model of dye. Although the photocatalytic activity of pure TiO_2 was found to be higher than that of Co/TiO_2 samples under UV irradiation, the presence of 0.24% cobalt dopant in TiO_2 nanoparticles resulted in a photocatalyst with the highest activity under visible light.

Keywords: TiO_2 nanoparticle; Cobalt; Photocatalytic degradation; Methylene blue

1. Introduction

Environmental cleaning using TiO_2 photocatalysts has attracted a great deal of attention due to the increase in the level of environmental pollutions in the world [1]. TiO_2 is considered as one of the most promising materials due to its high stability and environmental safety. However, the application of TiO_2 in water and air purification is restricted as its intrinsic wide band gap (3.2 eV) requires high energy excitation such as UV irradiation, which only composes 5% of solar irradiation. Thus, the major portion of solar energy (visible light) could not be used for photocatalytic reaction. Besides, high recombination rate of photo-excited carriers is another limitation for the applicable fields of TiO_2. Due to the short life of photo-excited carriers, only a small part of electrons and vacancies can move to its surface, which lead to further reduction of photocatalytic efficiency [2]. For more than a decade, studies have mainly concentrated on the suspension of TiO_2 fine powder because of its higher photocatalytic activity compared with TiO_2 thin films [3]. From among the three principal crystalline forms of titania, rutile does absorb some visible light, while anatase absorbs only in the UV region. Unfortunately, rutile is not a good photocatalyst. It is also known that optimal photocatalytic efficiency is obtained with a mixture of anatase and a small percentage of rutile [4]. Many attempts have been made to sensitize titanium dioxide to the whole visible region, such as doping with transition metals [5–16], transition metal ions [17–23], nonmetal atoms [13,24,25] and organic materials [26,27]. Introduction of dopants allows titania to absorb in the visible region but this does not necessarily mean that the doped catalyst has a better photocatalytic activity. When the doping level exceeds an optimal limit, which usually lies at very low dopant concentration and low visible light absorption, the dopant causes recombination of sites and has undesirable effects on photocatalysis [4].

* Corresponding author.

The sol-gel method is an attractive method for low-temperature synthesis of TiO_2, and it is easier to realize metal doping [10]. Since this method is carried out in solution, this permits tailoring of certain desired structural characteristics such as compositional homogeneity, grain size, particle morphology and porosity. Preparation of transition metal-doped TiO_2 nanoparticles by sol-gel method, characterization and investigation of their photocatalytic activity have been reported in recent literature [28,29].

To the best of knowledge, the application of TiO_2 nanoparticles containing different amounts of cobalt for heterogeneous photocatalytic degradation of methylene blue (MB) has not been reported so far. MB is the most commonly used substance for dying cotton, wood and silk. It can cause eye burns, which may be responsible for permanent injury to the eyes of human and animals. Although MB is seen in some medical uses in large quantities, it can also be widely used in coloring paper, dyeing cottons, wools, coating for paper stocks, etc. Though MB is not strongly hazardous, it can cause some harmful effects. Acute exposure to MB will cause increased heart rate, vomiting, shock, Heinz body formation, cyanosis, jaundice and quadriplegia and tissue necrosis in humans [25].

The aim of this work is that the cobalt doped to TiO_2 nanoparticles with photocatalytic activity were synthesized by sol-gel method. The as-prepared sample was characterized by X-ray diffraction (XRD), Fourier infrared spectroscopy (FTIR), scanning electron microscopy/energy dispersive X-ray (SEM/EDX), diffuse reflectance spectroscopy (DRS) and N_2 physisorption. The point of zero charge (PZC) of prepared photocatalysts was measured. Moreover, the photocatalytic performance of the prepared samples in degrading MB dye was estimated using UV–Vis spectrophotometry.

2. Experimental

2.1. Materials and reagents

Cobalt (II) chloride hexahydrate ($CoCl_2.6H_2O$) was supplied by Merck (Germany) (No. 102539). Tetraisopropylorthotitanat (Merck; No. 8.21895), ethanol, acetylacetone and deionized water were used for photocatalytic synthesis. High-purity MB (Merck, No. 115943) was used as a probe molecule for catalytic tests.

2.2. Photocatalyst preparation

Pure TiO_2 and TiO_2 photocatalyst containing different amounts of cobalt were synthesized by sol-gel method. In a typical reaction, a mixture of 20 mL $Ti(OC_3H_7)_4$, 20 mL ethanol and 1.62 mL acetylacetone was prepared and stirred for 30 min at room temperature. Then, a new mixture containing X mg $CoCl_2.6H_2O$ (X: 30, 60, 120 and 180 mg), 80 mL ethanol and 2 mL H_2O was added into the first solution, which led to a colored solution. This solution was transferred into an autoclave, and then heated to 240°C at a heating rate of about 2°C min^{-1}. Finally, the temperature was kept at 240°C for 6 h. After cooling, the obtained solid washed with ethanol and water and dried at 100°C for 2 h in air. These photocatalysts are labelled as Co/TiO_2 (a), where (a) is the weight percentage of cobalt in the final solid that obtained by EDX analysis. A solution without $CoCl_2.6H_2O$ was also prepared to obtain a control sample. This photocatalyst contains only TiO_2 prepared by an identical procedure.

2.3. Characterization

FTIR analysis was applied to determine the surface functional groups, using FTIR spectroscope (FTIR-2000, Bruker, USA), where the spectra were recorded from 4,000 to 400 cm^{-1}. The XRD patterns were recorded on a Siemens, D5000 (Germany). X-ray diffractometer using Cu Kα radiation as the X-ray source. The diffractograms were recorded in the 2θ range of 10°–70°. The morphology of nanoparticles were characterized using SEM (Vegall-Tescan Company, Czech Republic) equipped with an EDX. The diffuse reflectance UV–Vis spectra of the samples were recorded by an Ava Spec-2048TEC spectrometer. The nitrogen physisorption measurements were carried out with a Quantachrome Autosorb-1-MP. The Brunaur-Emmet-Teller (BET) areas were determined by static nitrogen physisorption at –196°C subsequent to outgassing at 250°C, until the pressure was lower than 5 mbar.

2.4. Study on point of zero charge

In the PZC (pH) determination, 0.01 M NaCl was prepared, and its pH was adjusted in the range of 2–11 by adding 0.01 M NaOH or HCl. Then, 50 mL of 0.01 M NaCl each was put in conical flask, and then 0.1 g of prepared samples was added to these solutions. These flasks were kept for 72 h, and final pH of the solution was measured by using pH meter. Graphs were then plotted for pH_{final} vs. $pH_{initial}$.

2.5. Photocatalytic degradation of MB

In a typical run, the suspension containing 10 mg photocatalyst and 100 mL aqueous solution of MB (10 mg/L) was stirred first for 60 min in the dark to establish adsorption/desorption equilibrium. Irradiation experiments were carried out in a self-built reactor. UV illumination was performed with a 400 W Kr lamp (Osram, Germany). The illumination power of the lamp is mainly in the UV-A region, that is, about 90% of the radiated power is in the UV-A region (400–315 nm) and about 10% in the UV-B region (315–280 nm). A visible (Halogen, ECO Osram, 500 W) lamp was used as alternative irradiation source. At certain intervals, small aliquots (2 mL) were withdrawn and filtered to remove the photocatalyst particles. These aliquots were used for monitoring the degradation progress, with Rayleigh UV-2601 UV–Vis spectrophotometer.

3. Results and discussion

3.1. XRD analysis

The XRD patterns of the prepared samples were shown in Fig. 1. The nanocrystalline anatase structure was confirmed by (1 0 1), (0 0 4), (2 0 0), (1 0 5) and (2 1 1) diffraction peaks [30]. The XRD patterns of anatase have a main diffractions at 2θ = 25.2° corresponding to the 101 plane (JCPDS 21-1272) while the main diffractions of rutile and brookite phases are at 2θ = 27.4° (110 plane) and 2θ = 30.8°

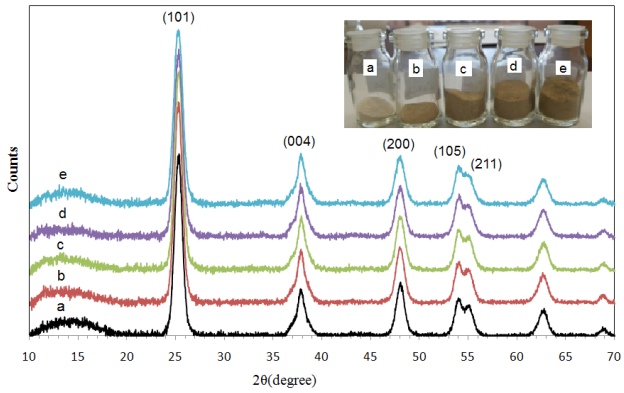

Fig. 1. Powder XRD patterns of: (a) TiO_2, (b) Co/TiO_2 (0.24), (c) Co/TiO_2 (0.30), (d) Co/TiO_2 (0.60) and (e) Co/TiO_2 (0.63).

(121 plane), respectively. Therefore, rutile and brookite phases have not been detected [31,32]. The XRD patterns of Co/TiO_2 samples didn't show any cobalt phase indicating that cobalt ions uniformly dispersed among the anatase crystallites [2,33–35]. Also, the shape of diffraction of pure TiO_2 is quite similar to that of Co/TiO_2 samples. It is deserve to be mentioned that the color of pure TiO_2 is white; however, Co/TiO_2 samples are all pale yellow, and the color is deepened when cobalt concentration is elevated (Fig. 1). For no peaks corresponding to metallic cobalt or cobalt compound is observed and the color of TiO_2 is changed with cobalt amount, it is reasonable to suppose that cobalt cations are successfully introduced into TiO_2 and homogenously distributed in the lattice of TiO_2. The diffraction patterns of pure TiO_2 and Co/TiO_2 samples show considerable line width, indicating small particles. The particle size of each sample is calculated from the full width at half maximum (FWHM) of the (101) diffraction peak using Scherrer's equation [36]:

$$D = K\lambda/\beta \cos\theta \quad (1)$$

where D is the crystal size of the sample; λ is the X-ray wavelength (1.54056 Å); β is the FWHM of the diffraction peak (radian); K is a coefficient (0.89) and θ is the diffraction angle at the peak maximum. The results are demonstrated in Table 1. All prepared samples are in nano-size range, from 14.38 to 16.53 nm, and all Co/TiO_2 samples except Co/TiO_2 (0.63) show larger crystal size compared with pure TiO_2. The increased particle size may be explained by the fact that the ionic radius of Co^{2+} (0.745 A°) is greater than that of Ti^{4+} (0.605 A°) [37]. In the case of Co/TiO_2 (d) sample, it can be concluded that the addition of cobalt to titania hinders the growth of TiO_2 nanoparticles. It seems that cobalt ions form complex with the TiO_2 surface oxygen, hence, suppress the growth of TiO_2 crystallite [38].

The lattice parameters (a = b ≠ c) were obtained for (101) crystal plane of anatase phase, according to the following equation (corresponding to tetragonal crystalline structure:

$$1/d^2 = (h^2 + k^2)/a^2 + l^2/c^2 \quad (2)$$

Table 1
Phase, crystal size and lattice parameters of prepared samples

Sample	Phase	Crystal size (nm)	a = b (Å)	c (Å)	Cell volume (Å^3)
TiO_2	Anatase	14.64	3.79	9.30	133.58
Co/TiO_2 (0.24)	Anatase	16.53	3.78	9.37	133.88
Co/TiO_2 (0.30)	Anatase	15.49	3.79	9.35	134.30
Co/TiO_2 (0.60)	Anatase	14.95	3.78	9.40	134.31
Co/TiO_2 (0.63)	Anatase	14.38	3.79	9.40	135.02

considering the interplanar spacing (d_{hkl}), the distance between adjacent planes in the set (hkl), can be determined using the Bragg Law:

$$d_{hkl} = \lambda/2 \sin\theta \quad (3)$$

The cell volume (tetragonal one) was determined as follows:

$$V = a^2c \quad (4)$$

where a and c are lattice parameters. Table 1 shows the lattice parameters of prepared samples.

The full pattern Rietveld refinement confirms that TiO_2 crystallizes in the anatase type of tetragonal structure. The obtained values of the lattice parameters for pure TiO_2 are in very good agreement with the anatase structure (Joint Committee for Powder Diffraction Standard, 78-2486) of TiO_2. No other impurity peaks are detected, which ensure high purity of TiO_2 powder used for Co doping. The diffraction patterns of prepared samples do not show any extra peaks confirming that the anatase phase is not disturbed upon Co doping in TiO_2. A significant difference between ionic radii of the dopant and the host ions (i.e., Co^{2+}: 0.745 Å and Ti^{4+}: 0.605 Å, with a coordination number of 6) is expected to cause a small enhancement of the TiO_2 unit cell size. In the refinement process, the Co occupancies were varied for the Ti and O sites to locate the exact positions of dopant atoms. Best fits were obtained when Co atoms occupy the Ti site with a total preference, while these atoms occupying the O site gave poor fits. These observations confirm that Co ions substitute the Ti site and have well been incorporated in host TiO_2 matrix. Furthermore, there is no sign of Co cluster phases thought the whole range of Co contents investigated so we can assertively rule out the presence of any impurity phase within the limits of such detection by XRD. Therefore, XRD patterns seem to provide evidence for the high homogeneity of doping and for the absence of secondary phases in the samples within the sensitivity of XRD.

3.2. SEM/EDX analysis

SEM micrographs of the TiO_2 and Co/TiO_2 samples are shown in Fig. 2. SEM images show that all the samples are slightly agglomerated, which it is more intense regarding to the doped samples compared with pure

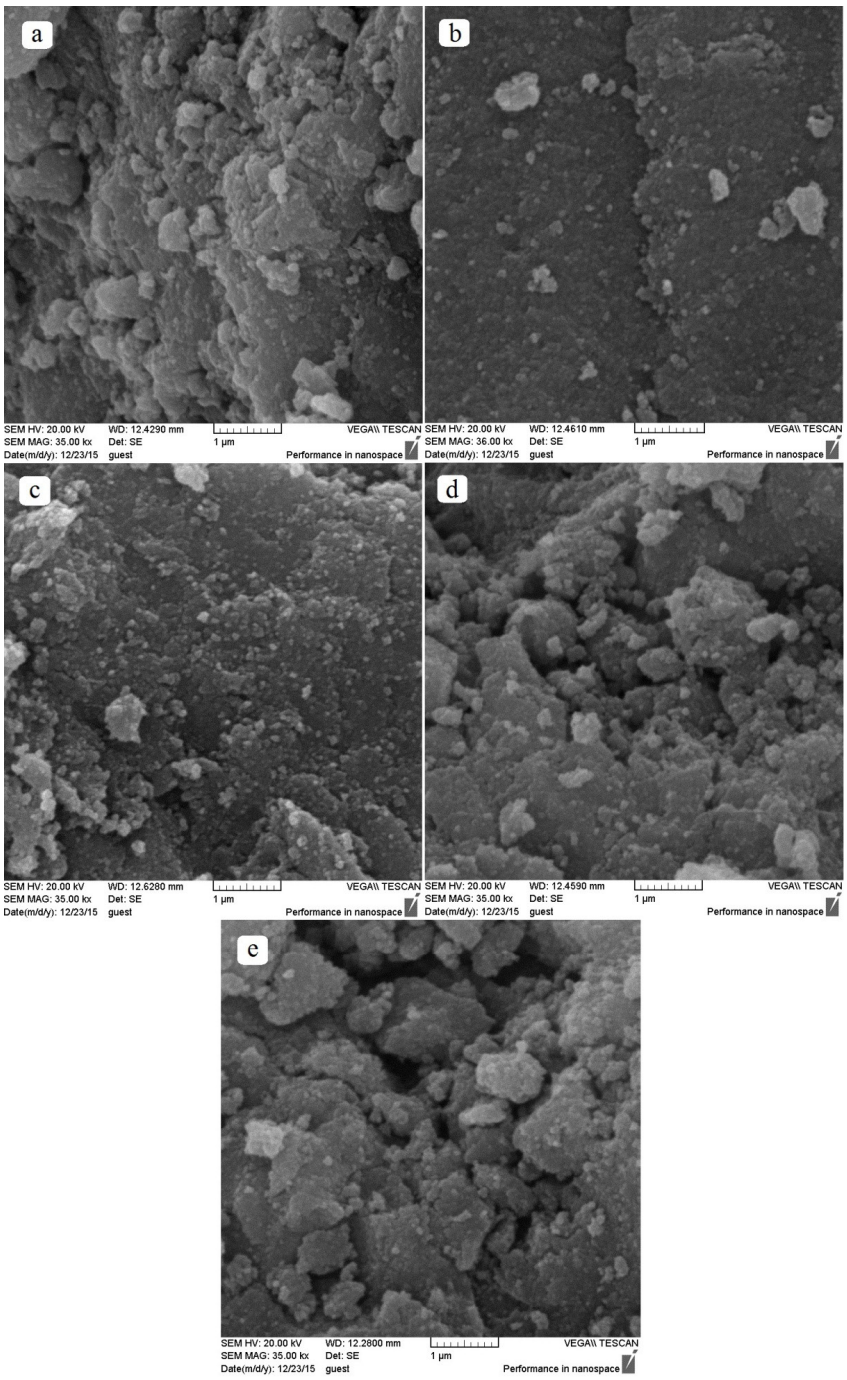

Fig. 2. SEM images of: (a) TiO_2, (b) Co/TiO_2 (0.24), (c) Co/TiO_2 (0.30), (d) Co/TiO_2 (0.60) and (e) Co/TiO_2 (0.63).

TiO_2 [39,40]. The EDX patterns of Co/TiO_2 samples in Fig. 3 show two peaks around 0.2 and 4.5 keV. The intense peak is assigned to the bulk TiO_2 and the less intense one to the surface TiO_2. The peaks of cobalt are distinct in Fig. 3 at 0.6, 6.9 and 7.5 keV. The less intense peak is assigned to cobalt in the TiO_2 lattices [20,38]. These results confirmed the existence of cobalt atoms in the Co/TiO_2 samples but the XRD patterns do not show any diffractions related to cobalt. Therefore, it may be concluded that cobalt ions are uniformly dispersed among the anatase crystallites. Fig. 4 shows (EDS) elemental mapping images of prepared samples. From the elemental mapping mode, highly and uniformly dispersed cobalt in the TiO_2 lattice was observed. This implies good interaction between cobalt and TiO_2 in the preparation process using the sol-gel method. The elemental analysis of Co/TiO_2 samples confirmed the presence of cobalt ions in the powder structure, as the opposite of XRD patterns. The XRD patterns do not show any diffractions related to cobalt presence in TiO_2 structure (EDS results are given in Table 2).

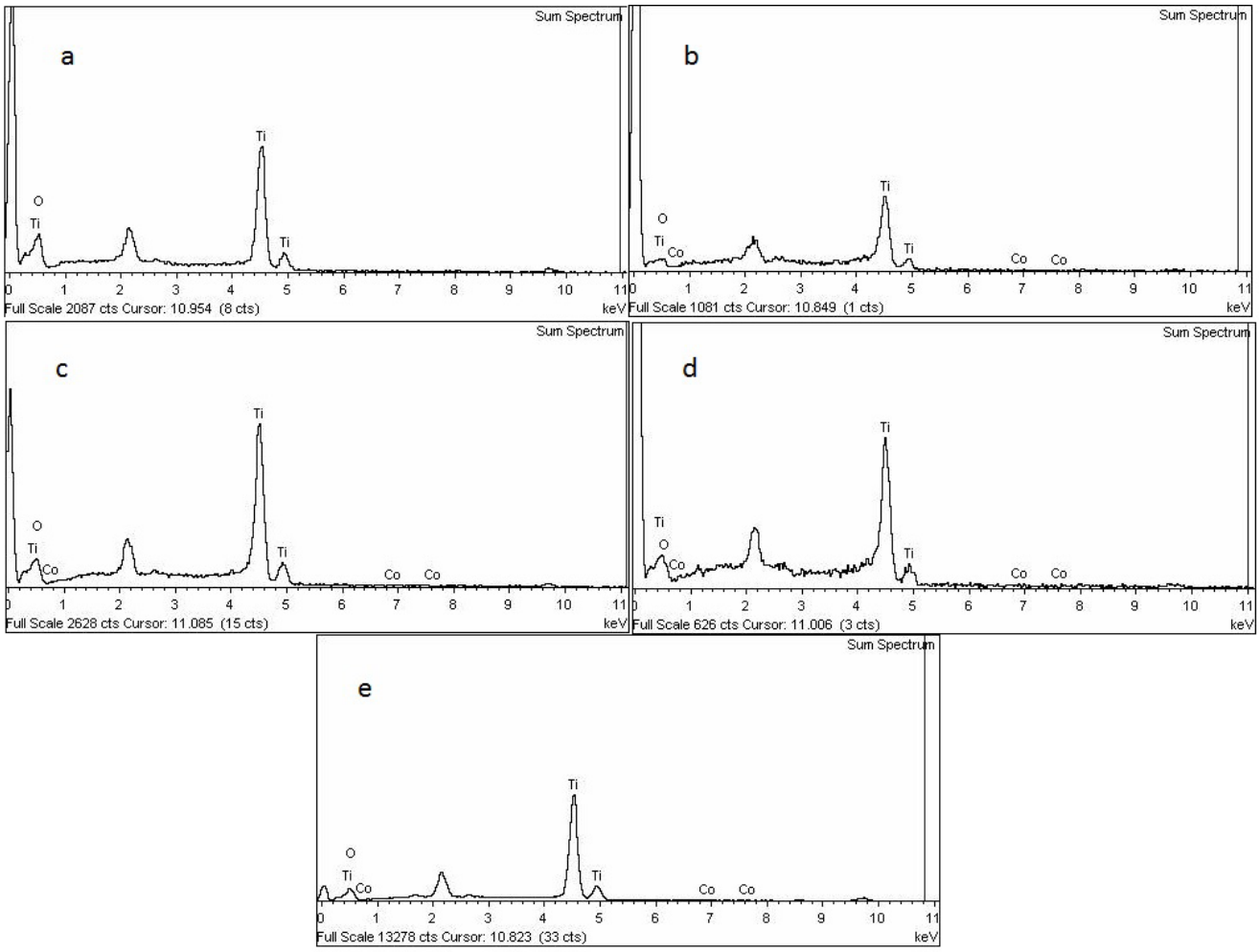

Fig. 3. EDX patterns of: (a) TiO_2, (b) Co/TiO_2 (0.24), (c) Co/TiO_2 (0.30), (d) Co/TiO_2 (0.60) and (e) Co/TiO_2 (0.63).

3.3. FTIR analysis

Fig. 5 shows the FTIR spectra of the TiO_2 and Co/TiO_2 samples. The peak positioned at 3,350–3,450 cm^{-1} is attributed to O–H stretching vibration. The peaks appearing at 1,620–1,635 cm^{-1} were attributed to H–O–H bending vibration mode of physically adsorbed water [41]. The broad intense band below 1,000 cm^{-1} is due to Ti-O-Ti vibrations. The surface hydroxyl groups in TiO_2 increase with the increase of cobalt loading, which is confirmed by increase in intensity of the corresponding peaks [38].

3.4. DRS analysis

DRS studies help to understand the band gaps of the material. The band gaps will change during the photoreaction as the catalysts are exposed to photons of different energies. The chemistry involved can be highlighted by these changes [42]. The diffuse reflectance spectra of prepared samples are shown in Fig. 6. The Diffuse Reflectance (DR) spectrum of TiO_2 consists of a broad intense absorption around 400 nm, due to the charge-transfer from the valence band formed by 2p orbitals of the oxide anions to the conduction band formed by 3d t_{2g} orbitals of the Ti^{4+} cations [38]. DR spectra of Co/TiO_2 samples showed a redshift in the absorption value. Increase in the concentration of cobalt ions on TiO_2 resulted in a prominent change or shift of band edge from UV to visible region. The DR spectra of the Co/TiO_2 samples consist of additional absorption peaks in the range of 500–650 nm. With the gradual increase of Co^{2+} concentration on TiO_2, the sharpness and intensity of absorption band between 500 and 650 nm are also increased gradually [43]. The genesis of absorption peak that is increasing with cobalt concentration in TiO_2 is attributed to Co^{2+}/Ti^{4+} charge-transfer interaction. This may also be a reason for high photoactivity of these materials in the visible region.

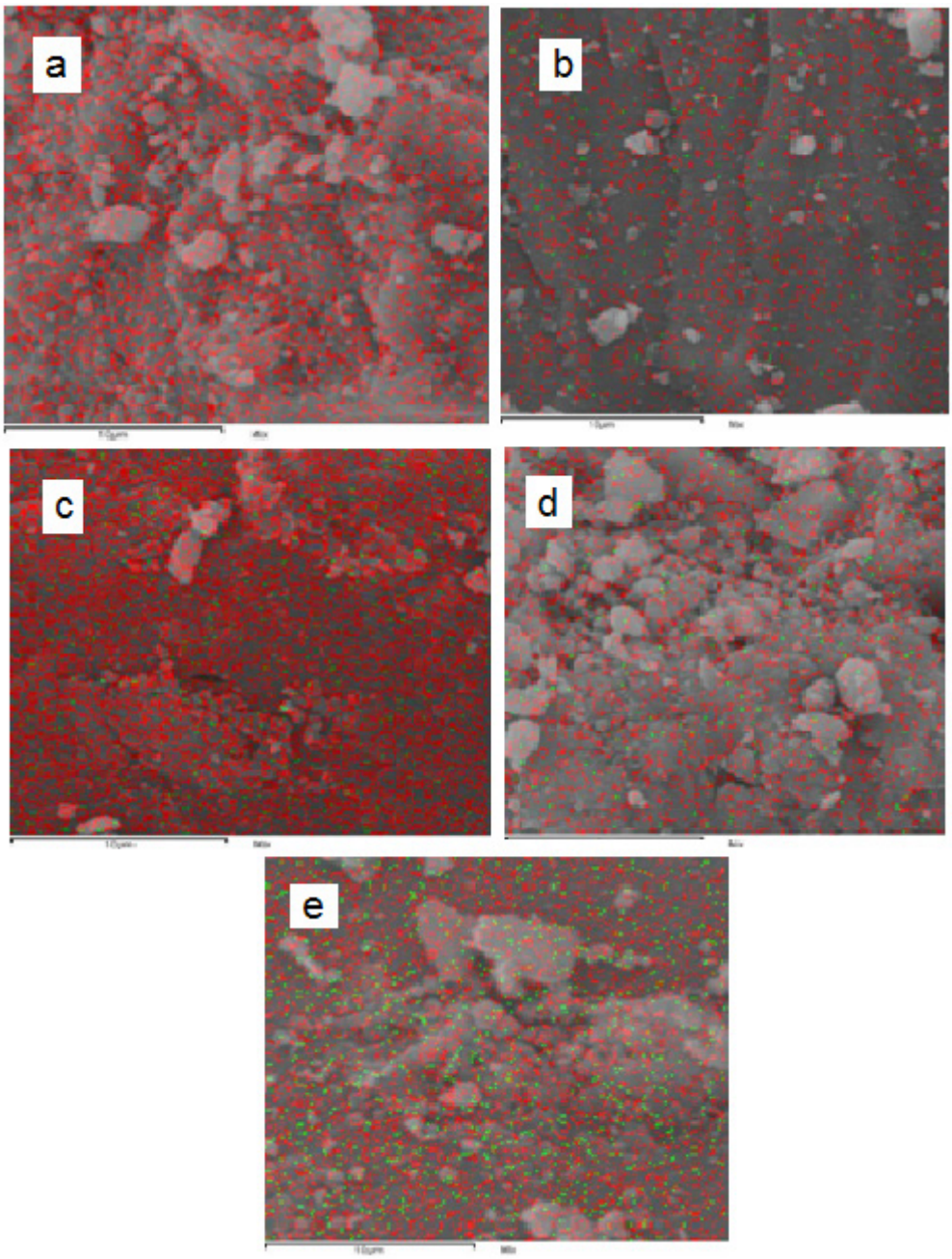

Fig. 4. EDS analysis (elemental mapping images) of: (a) TiO_2, (b) Co/TiO_2 (0.24), (c) Co/TiO_2 (0.30), (d) Co/TiO_2 (0.60) and (e) Co/TiO_2 (0.63).

Table 2
Elemental chemical analysis of the prepared samples

Sample	% Co	% Ti	% O
TiO_2	0.00	62.20	37.80
Co/TiO_2 (0.24)	0.24	51.38	48.37
Co/TiO_2 (0.30)	0.30	47.12	52.58
Co/TiO_2 (0.60)	0.60	46.73	52.67
Co/TiO_2 (0.63)	0.63	51.03	48.34

We calculated the band gap energy from the DR spectra according to below equation [44] for the pure TiO_2 and Co/TiO_2 samples:

$$E_{bg} = 1{,}240/\lambda \quad (5)$$

where E_{bg} is the band gap energy (eV), and λ is wavelength (nm) obtained from the DR spectra. The E_{bg} data of samples are summarized in Table 3. The band gap of all Co/TiO_2 samples decreased slightly compared with TiO_2 (Table 3). But for all the Co/TiO_2 samples, the absorption efficiencies in

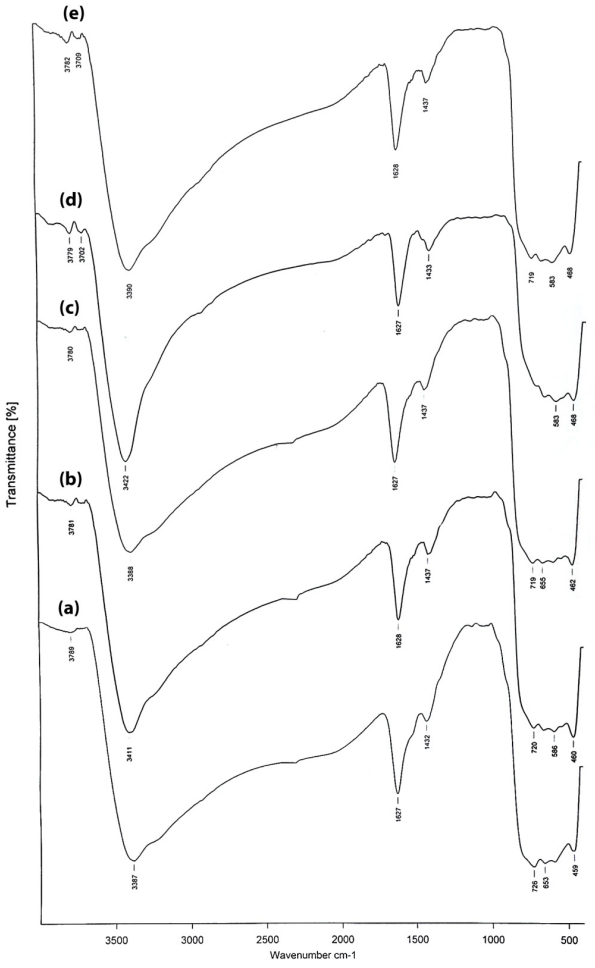

Fig. 5. FTIR spectra of: (a) TiO_2, (b) Co/TiO_2 (0.24), (c) Co/TiO_2 (0.30), (d) Co/TiO_2 (0.60) and (e) Co/TiO_2 (0.63).

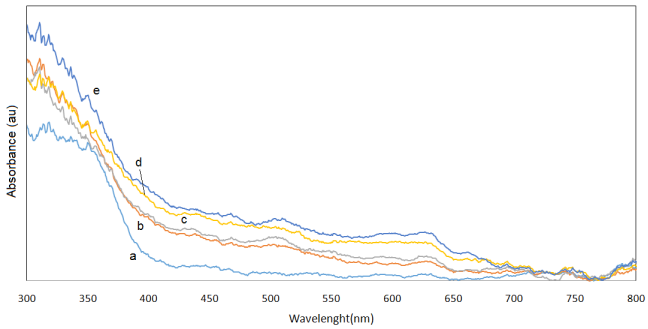

Fig. 6. Diffuse reflectance spectra of: (a) TiO_2, (b) Co/TiO_2 (0.24), (c) Co/TiO_2 (0.30), (d) Co/TiO_2 (0.60) and (e) Co/TiO_2 (0.63).

the range of 400–700 nm are improved, and the increment is proportional to the cobalt amount [38].

3.5. Point of zero charge

Oxide surfaces can become charged as a consequence of the ability of coordinated OH groups to undergo hydrolysis. Thus, negatively and positively charged surfaces are obtained by the dissociation of acid groups and protonation of basic groups, respectively. The PZC, corresponding to the condition where no net charge is present on the surface, is an important factor that controls the adsorption of solution species and photocatalytic activity [45]. For undoped TiO_2, the pH value of the PZC is 7.10, and for the Co-doped TiO_2 samples, the pH is shifted to higher pH values. Thus, the PZC seems to approach that of bulk Co_3O_4 [46], and one would be led to consider this as a possible cause; it can be ruled out, however, since our DRS and XRD measurements do not indicate the presence of Co^{3+} and of any separate phase formation for Co amounts <1%. Quite obviously, the phenomenon we observed originates from changes in the surface properties that can be even rather subtle, as pointed out in an illuminating work by Contescu et al. on heterogeneity of hydroxyl groups on TiO_2 polymorphs [47]. Among other factors, differences in coordination of –O- and –OH sites to cations, a different proportion of proton binding groups (oxo and hydroxo), variation of the proton-metal distances, and the contribution of different crystal planes (on different planes, terminal oxygen has different acidity) can bring about observable changes in the surface acid/basic behavior. In contrast to relatively abundant information available for pure TiO_2, investigations on doped TiO_2 appear scanty [45]. From our X-ray data, we have neither evidence of changes in the crystallographic planes intensity upon cobalt incorporation nor evidence of changes in the TiO_2 unit cell parameters. In this regard, it is worth stressing that Geng and Kim [48] showed that the introduction of interstitial Co into $Ti_{16}O_{32}$ model clusters leads to volume expansion, and an increased Ti–O bond length can then possibly lead to a more basic behavior of the surface as discussed by Contescu et al. [47]. Table 4 shows PZC (pH) for our synthesized samples.

Table 3
Color, wavelength and band gap energy of the prepared samples

Sample	Color	λ (nm)	Band gap energy (eV)
TiO_2	White	400	3.10
Co/TiO_2 (0.24)	Pale yellow	412	3.01
Co/TiO_2 (0.30)	Yellow	414	3.00
Co/TiO_2 (0.60)	Dark yellow	416	2.98
Co/TiO_2 (0.63)	Dark yellow	416	2.98

Table 4
Point of zero charge (PZC) (pH) of the prepared samples

Sample	PZC (pH)
TiO_2	7.10
Co/TiO_2 (0.24)	7.40
Co/TiO_2 (0.30)	7.50
Co/TiO_2 (0.60)	7.62
Co/TiO_2 (0.63)	7.65

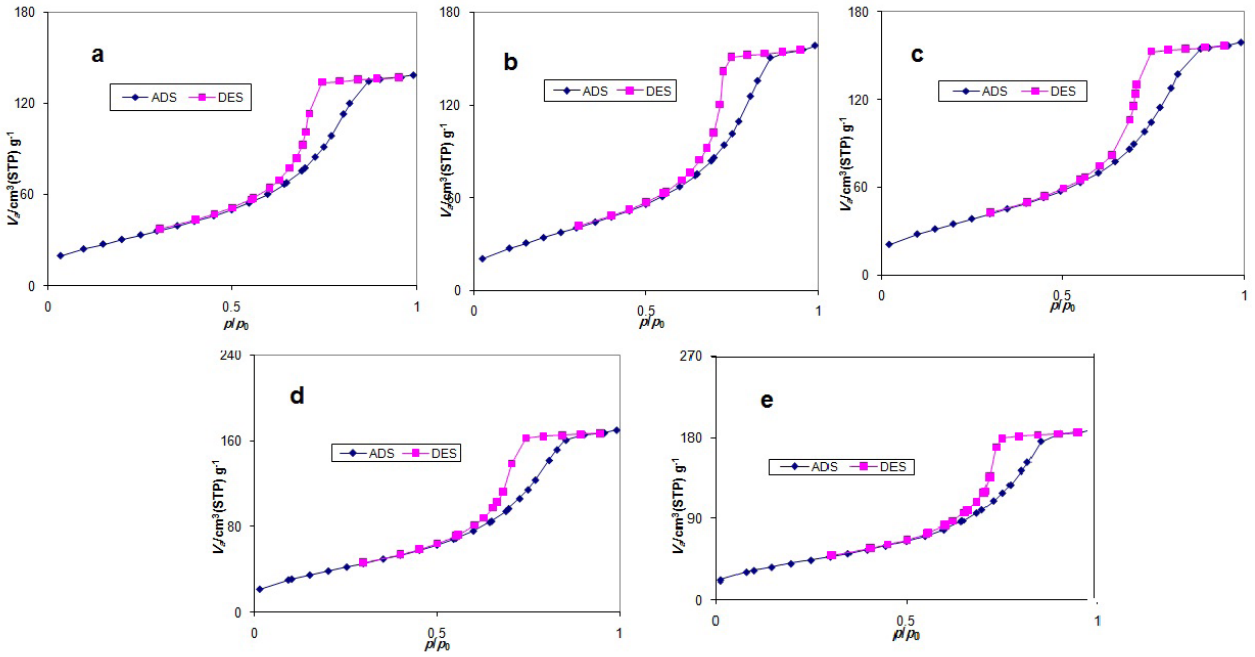

Fig. 7. N_2 adsorption–desorption isotherms for: (a) TiO_2, (b) Co/TiO_2 (0.24), (c) Co/TiO_2 (0.30), (d) Co/TiO_2 (0.60) and (e) Co/TiO_2 (0.63).

3.6. N_2 adsorption–desorption

Fig. 7 shows N_2 adsorption–desorption isotherms of the synthesized photocatalysts. The sorption isotherms in Fig. 7 correspond to the type IV isotherm according to the International Union of Pure and Applied Chemistry (IUPAC) classification [49]. Textural and structural parameters of the Co/TiO_2 samples are summarized in Table 5. Specific surface areas and average pore diameter were calculated according to the BET method; pore volumes were derived from the desorption branch according to the Barrett-Joyner-Halenda (BJH) model. A considerable increase in the value of surface area and decrease in the crystallite size are seen with the increase of Co-dopant concentration in TiO_2. The increase of surface area and decrease of crystallite size with the introduction of any foreign material in TiO_2 is a general phenomenon and is expected to be due to the prevention of agglomeration of TiO_2 particles by the incorporated material [38,50–55].

3.7. Photocatalytic degradation of MB

The results of photocatalytic degradation of MB under UV irradiation and visible light are shown in Figs. 8 and 9. Under UV irradiation, pure TiO_2 shows better results than Co/TiO_2 samples. It seems that among the Co/TiO_2 samples, the sample containing 0.24% cobalt has the best performance. It was also observed that pure TiO_2 degraded 100% MB after 150 min irradiation while the 0.24% Co/TiO_2 did it (~80% degradation) after 150 min irradiation. Under visible light, the best degradation of MB was achieved in the presence of 0.24% Co/TiO_2, which decomposed 62% of MB after 150 min. The two basic factors that are responsible for the activity of photocatalysts include surface area and light absorption capacity [38]. The DRS analysis

Table 5
Textural and structural parameters of the prepared samples

Sample	S_{BET} (m^2/g)	Average pore diameter (nm)	Pore volume (cm^3/g)
TiO_2	116.651	7.339	0.222
Co/TiO_2 (0.24)	130.900	7.476	0.253
Co/TiO_2 (0.30)	135.810	7.232	0.254
Co/TiO_2 (0.60)	145.310	7.224	0.271
Co/TiO_2 (0.63)	151.661	7.755	0.302

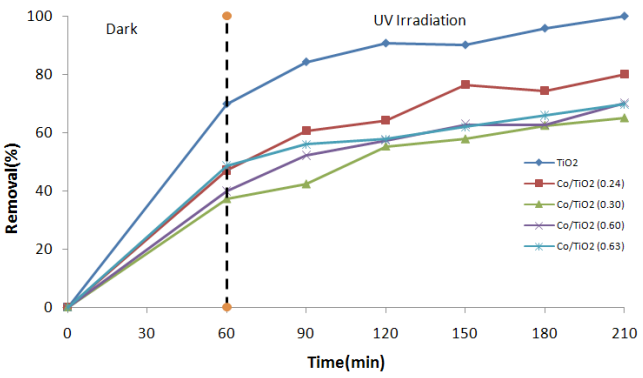

Fig. 8. Photocatalytic degradation of MB in the presence of prepared samples under UV irradiation: initial concentration of MB, 10 mg /L; volume, 100 mL; pH, 9 and catalyst dosage, 10 mg.

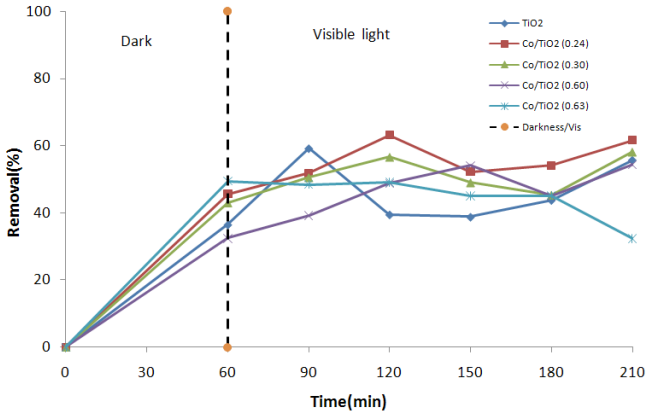

Fig. 9. Photocatalytic degradation of MB in the presence of prepared samples under visible light: initial concentration of MB, 10 mg /L; volume, 100 mL; pH, 9 and catalyst dosage, 10 mg.

results (Fig. 6) show that light absorption capacities of the prepared samples are different and increase with an increase in the cobalt amount in visible region. Therefore, increasing the cobalt amount has two opposite effects on the photocatalytic activity of the Co/TiO_2 samples; increasing light absorption capacity and decreasing surface area. The photocatalytic activity depends on which one of these is the dominant factor. A lesser amount of surface hydroxyl groups was observed in the case of Co/TiO_2 samples compared with the undoped TiO_2. This could be one of the reasons for the lower activity of the metal-doped TiO_2 catalysts. Most of the metal-doped TiO_2 samples absorb in the visible region. It should be noted that the degradation rates in the presence of Co-doped TiO_2 catalysts under UV irradiation were in general less than that of the undoped TiO_2. Recombination of photogenerated electrons and holes is one of the most significant factors that deteriorate the photoactivity of the TiO_2 catalyst. Any factor that suppresses the electron-hole recombination will therefore enhance the photocatalytic activity [56,57]. Perhaps, cobalt particles are sites for recombination of the generated electron-holes and, hence, decrease the photocatalytic activity. Also, it is reported [58] that the optimal concentration of doping ions should make the thickness of the space charger layer substantially equal to the light penetration depth. Therefore, further addition of cobalt leads to gradually reduction of catalytic efficiency.

4. Conclusion

TiO_2-based photocatalysts containing different amounts of cobalt were synthesized and characterized by several techniques successfully. XRD analysis confirmed all the prepared samples consist of pure anatase phase. The XRD, SEM/EDX, DRS and N_2 physisorption data showed that the incorporation of cobalt in TiO_2 network increases the nanoparticles size, shifts the absorption edge to higher wavelengths (red-shift) and higher the surface area of the particles. The photocatalytic degradation of MB under UV irradiation revealed higher activity in the presence of the pure TiO_2 than the Co/TiO_2 samples. Among the Co/TiO_2 samples, the Co/TiO_2 (0.24) photocatalyst exhibited the highest photocatalytic activity under visible light.

Acknowledgments

The author wish to acknowledge the financial support of Iran National Science Foundation (Grant No.: 92025598). Also, I am so thankful to University of Tehran for supporting of this research.

References

[1] F.A. Fujishima, T.N. Rao, D.A. Tryk, Titanium dioxide photocatalysis, J. Photochem. Photobiol., C, 1 (2000) 1–21.
[2] P. Jiang, W. Xiang, J. Kuang, W. Liu, W. Cao, Effect of cobalt doping on the electronic, optical and photocatalytic properties of TiO_2, Solid State Sci., 46 (2015) 27–32.
[3] Y. Jiaguo, C.Y.U. Jimmy, B. Cheng, X. Zhao, Photocatalytic activity and characterization of the sol-gel derived Pb-doped TiO_2 thin films, J. Sol-Gel Sci. Technol., 24 (2002) 39–48.
[4] P. Bouras, E. Stathatos, P. Lianos, Pure versus metal-ion-doped nanocrystalline titania for photocatalysis, Appl. Catal., B, 73 (2007) 51–59.
[5] F. Sayilkan, M. Asilturk, P. Tatar, N. Kiraz, S. Sener, E. Arpac, H. Sayilkan, Photocatalytic performance of Sn-doped TiO_2 nanostructured thin films for photocatalytic degradation of malachite green dye under UV and VIS-lights, Mat. Res. Bull., 43 (2008) 127–134.
[6] J. Liqiang, S. Xiaojun, X. Baifu, W. Baiqi, C. Weimin, F. Honggang, The preparation and characterization of La doped TiO_2 nanoparticles and their photocatalytic activity, J. Solid State Chem., 177 (2004) 3375–3382.
[7] M. Kang, Synthesis of Fe/TiO_2 photocatalyst with nanometer size by solvothermal method and the effect of H_2O addition on structural stability and photodecomposition of methanol, J. Mol. Catal. A: Chem., 197 (2003) 173–183.
[8] B.Y. Lee, S.H. Park, M. Kang, S.C. Lee, S.J. Choung, Preparation of Al/TiO_2 nanometer photo-catalyst film and the effect of H_2O addition on photo-catalytic performance for benzene removal, Appl. Catal., A, 253 (2003) 371–380.
[9] M.K. Seery, R. George, P. Floris, S.C. Pillai, Silver doped titanium dioxide nanomaterials for enhanced visible light photocatalysis, J. Photochem. Photobiol., A, 189 (2007) 258–263.
[10] J. Zhou, Y. Zhang, X.S. Zhao, A.K. Ray, Photodegradation of benzoic acid over metal-doped TiO_2, Ind. Eng. Chem. Res., 45 (2006) 3503–3511.
[11] S.S. Lee, H.J. Kim, K.T. Jung, H.S. Kim, Y.G. Shul, Photocatalytic activity of metal ion (Fe or W) doped titania, Korean J. Chem. Eng., 18 (2001) 914–918.
[12] N. Sobana, M. Muruganadham, M. Swaminathan, Nano-Ag particles doped TiO_2 for efficient photodegradation of direct azo dyes, J. Mol. Catal. A: Chem., 258 (2006) 124–132.
[13] J.C.S. Wu, C.H. Chen, A visible-light response vanadium-doped titania nanocatalyst by sol–gel method, J. Photochem. Photobiol., A, 163 (2004) 509–515.
[14] M. Subramanian, S. Vijayalakshmi, S. Venkataraj, R. Jayavel, Effect of cobalt doping on the structural and optical properties of TiO_2 films prepared by sol–gel process, Thin Solid Films, 516 (2008) 3776–3782.
[15] Y. Yang, X. Li, J. Chen, L. Wang, Effect of doping mode on the photocatalytic activities of Mo/TiO_2, J. Photochem. Photobiol., A, 163 (2004) 517–522.
[16] J. Lee, W. Choi, Effect of platinum deposits on TiO_2 on the anoxic photocatalytic degradation pathways of alkylamines in water: dealkylation and N-alkylation, Environ. Sci. Technol., 38 (2004) 4026–4033.
[17] S. Kim, S. Hwang, W. Choi, Visible light active platinum-ion-doped TiO_2 photocatalyst, J. Phys. Chem. B, 109 (2005) 24260–24267.
[18] Y. Wang, H. Cheng, L. Zhang, Y. Hao, J. Ma, B. Xu, W. Li, The preparation, characterization, photoelectrochemical and photocatalytic properties of lanthanide metal-ion-doped TiO_2 nanoparticles, J. Mol. Catal. A: Chem., 151 (1999) 205–216.

[19] W. Hung, S. Fu, J. Tseng, H. Chu, T. Ko, Study on photocatalytic degradation of gaseous dichloromethane using pure and iron ion-doped TiO_2 prepared by the sol–gel method, Chemosphere, 66 (2007) 2142–2151.
[20] N. Venkatachalam, M. Palanichamy, B. Arabindoo, V. Murugesan, Enhanced photocatalytic degradation of 4-chlorophenol by Zr^{4+} doped nano TiO_2, J. Mol. Catal. A: Chem., 266 (2007) 158–165.
[21] J. Zhou, M. Takeuchi, A.K. Ray, M. Anpo, X.S. Zhao, Enhancement of photocatalytic activity of P25 TiO_2 by vanadium-ion implantation under visible light irradiation, J. Colloid Interface Sci., 311 (2007) 497–501.
[22] Y. Zhang, H. Zhang, Y. Xu, Y. Wang, Europium doped nanocrystalline titanium dioxide: preparation, phase transformation and photocatalytic properties, J. Mater. Chem., 13 (2003) 2261–2265.
[23] J. Chen, M. Yao, X. Wang, Investigation of transition metal ion doping behaviors on TiO_2 nanoparticles, J. Nanopart. Res., 10 (2008) 163–171.
[24] S. Liu, X. Chen, A visible light response TiO_2 photocatalyst realized by cationic S-doping and its application for phenol degradation, J. Hazard. Mater., 152 (2008) 48–55.
[25] M. Crisan, A. Braileanu, M. Raileanu, M. Zaharescu, D. Crisan,N. Dragan, M. Anastasescu, A. Ianculescu, I. Nitoi, V.E.Marinescu, S.M. Hodorogea, TiO_2-based nanomaterials with photocatalytic properties for the advanced degradation of xenobiotic compounds from water. A literature survey, Water, Air , Soil Pollut., 224 (2013) 1–45.
[26] D. Jiang, Y. Xu, B. Hou, D. Wu, Y. Sun, Synthesis of visible light-activated TiO_2 photocatalyst via surface organic modification, J. Solid State Chem., 180 (2007) 1787–1791.
[27] R.S. Sonawane, B.B. Kale, M.K. Dongare, Preparation and photo-catalytic activity of Fe–TiO_2 thin films prepared by sol–gel dip coating, Mater. Chem. Phys., 85 (2004) 52–57.
[28] N. Venkatachalam, M. Palanichamy, V. Murugesan, Sol–gel preparation and characterization of alkaline earth metal doped nano TiO_2: efficient photocatalytic degradation of 4-chlorophenol, J. Mol. Catal. A: Chem., 273 (2007) 177–185.
[29] H. Luo, C. Wang, Y. Yan, Synthesis of mesostructured titania with controlled crystalline framework, Chem. Mater., 15 (2003) 3841–3846.
[30] H. Ogawa, A. Abe, Preparation of tin oxide films from ultrafine particles, J. Electrochem. Soc., 128 (1981) 685–689.
[31] K.V. Baiju, P. Shajesh, W. Wunderlich, P. Mukundan, S.R. Kumar, K.G.K. Warrier, Effect of tantalum addition on anatase phase stability and photoactivity of aqueous sol–gel derived mesoporous titania, J. Mol. Catal. A: Chem., 276 (2007) 41–46.
[32] K.M.K. Srivatsa, M. Bera, A. Basu, Pure brookite titania crystals with large surface area deposited by plasma enhanced chemical vapour deposition technique, Thin Solid Films, 516 (2008) 7443–7446.
[33] Q. Chen, F. Ji, T. Liu, P. Yan, W. Guan, X. Xu, Synergistic effect of bifunctional Co–TiO_2 catalyst on degradation of Rhodamine B: Fenton-photo hybrid process, Chem. Eng. J., 229 (2013) 57–65.
[34] T. Preethi, B. Abarna, K.N. Vidhya, G.R. Rajarajeswari, Sol–gel derived cobalt doped nano-titania photocatalytic system for solar light induced degradation of crystal violet, Ceram. Int., 40 (2014) 13159–13167.
[35] A. Kaushi, B. Dalela, S. Kumar, P.A. Alvi, S. Dalela, Role of Co doping on structural, optical and magnetic properties of TiO_2, J. Alloys Compd., 552 (2013) 274–278.
[36] M. Khan, W. Cao, Cationic (V, Y)-codoped TiO_2 with enhanced visible light induced photocatalytic activity: a combined experimental and theoretical study, J. Appl. Phys., 114 (2013) 183514.
[37] L. Xiu-Hua, H. Xiao-Bo, F. Yi-Bei, Effects of doping cobalt on the structures and performances of TiO_2 photocatalyst, Acta Chim. Sinica, 66 (2008) 1725–1730.
[38] M. Hamadanian, A. Reisi-Vanani, A. Majedi, Sol-gel preparation and characterization of Co/TiO_2 nanoparticles: application to the degradation of methyl orange, J. Iran. Chem. Soc., 7 (2010) 52–58.
[39] M. Hamadanian, A. Sadeghi Sarabi, A. Mohammadi Mehra, V. Jabbari, Photocatalyst Cr-doped titanium oxide nanoparticles: fabrication, characterization, and investigation of the effect of doping on methyl orange dye degradation, Mater. Sci. Semicond. Process, 21 (2014) 161–166.
[40] M. Hamadanian, V. Jabbari, M. Asad, M. Shamshiri, I. Mutlay, Preparation of novel hetero-nanostructures and high efficient visible light-active photocatalyst using incorporation of CNT as an electron-transfer channel into the support TiO_2 and PbS, J. Taiwan Inst. Chem. Eng., 44 (2013) 748–757.
[41] S. Mugundan, B. Rajamannan, G. Viruthagiri, N. Shanmugam, R. Gobi, P. Praveen, Synthesis and characterization of undoped and cobalt-doped TiO_2 nanoparticles via sol–gel technique, Appl. Nanosci., 5 (2015) 449–456.
[42] G. Sadanandam, K. Lalitha, V.D. Kumari, M.V. Shankar, M. Subrahmanyam, Cobalt doped TiO_2: a stable and efficient photocatalyst for continuous hydrogen production from glycerol: water mixtures under solar light irradiation, Int. J. Hydrogen Energy, 38 (2013) 9655–9664.
[43] I. Ganesh, A.K. Gupta, P.P. Kumar, P.S. Chandra Sekhar, K. Radha, G. Padmanabham, G. Sundararajan, Preparation and characterization of Co-doped TiO_2 materials for solar light induced current and photocatalytic applications, Mater. Chem. Phys., 135 (2012) 220–234.
[44] A. Kudo, Y. Miseki, Heterogeneous photocatalyst materials for water splitting, Chem. Soc. Rev., 38 (2009) 253–278.
[45] A. Di Paola, E. García-López, S. Ikeda, G. Marcì, B. Ohtani, L. Palmisano, Photocatalytic degradation of organic compounds in aqueous systems by transition metal doped polycrystalline TiO_2, Catal. Today, 75 (2002) 87–93.
[46] A. Daghetti, G. Lodi, S. Trasatti, Interfacial properties of oxides used as anodes in the electrochemical technology, Mater. Chem. Phys., 8 (1983) 1–90.
[47] C. Contescu, V.T. Popa, J.A. Schwarz, Heterogeneity of hydroxyl and deuteroxyl groups on the surface of TiO_2 polymorphs, J. Colloid Interface Sci., 180 (1996) 149–161.
[48] W.T. Geng, K.S. Kim, Interplay of local structure and magnetism in Co-doped TiO_2 anatase, Solid State Commun., 129 (2004) 741–746.
[49] K.S.W. Sing, D.H. Everett, R.A.W. Haul, L. Moscou, R.A. Pierotti, Reporting physisorption data for gas/solid systems with special reference to the determination of surface area and porosity, Pure Appl. Chem., 57 (1985) 603–619.
[50] M. Subramanian, S. Vijayalakshmi, S. Venkataraj, R. Jayavel, Effect of cobalt doping on the structural and optical properties of TiO_2 films prepared by sol–gel process, Thin Solid Films, 516 (2008) 3776–3782.
[51] Y.J. Lin, Y.H. Chang, W.D. Yang, B.S. Tsai, Synthesis and characterization of ilmenite $NiTiO_3$ and $CoTiO_3$ prepared by a modified Pechini method, J. Non-Cryst. Solids, 352 (2006) 789–794.
[52] G.W. Zhou, D.K. Lee, Y.H. Kim, C.W. Kim, Y.S. Kang, Preparation and spectroscopic characterization of ilmenite-type $CoTiO_3$ nanoparticles, Bull. Korean Chem. Soc., 27 (2006) 368–372.
[53] R.A. Oaxaca, J.J. Becerril, Titanium oxide modification with oxides of mixed cobalt valence for photocatalysis, J. Mex. Chem. Soc., 54 (2010) 164–168.
[54] B.M. Reddy, I. Ganesh, Characterization of La_2O_3-TiO_2 and V_2O_5/La_2O_3-TiO_2 catalysts and their activity for synthesis of 2,6-dimethylphenol, J. Mol. Catal. A: Chem., 169 (2001) 207–223.
[55] B.M. Reddy, I. Ganesh, E.P. Reddy, A. Fernández, P.G. Smirniotis, Surface characterization of Ga_2O_3–TiO_2 and V_2O_5/Ga_2O_3–TiO_2 catalysts, J. Phys. Chem. B, 105 (2001) 6227–6235.
[56] S. Sakthivel, M.V. Shankar, M. Palanichamy, B. Arabindoo, D.W. Bahnemann, V. Murugesan, Enhancement of photocatalytic activity by metal deposition: characterisation and photonic efficiency of Pt, Au and Pd deposited on TiO_2 catalyst, Water Res., 38 (2004) 3001–3008.
[57] K. Nagaveni, M.S. Hegde, G. Madras, Structure and photocatalytic activity of $Ti_{1-x}M_xO_{2\pm\delta}$ (M = W, V, Ce, Zr, Fe, and Cu) synthesized by solution combustion method, J. Phys. Chem. B, 108 (2004) 20204–20212.
[58] W. Zhou, Q. Liu, Z. Zhu, J. Zhang, Preparation and properties of vanadium-doped TiO_2 photocatalysts, J. Phys. D: Appl. Phys., 43 (2010) 035301.